1. Introduction

Mid-infrared (MIR) wavelengths between 2.5 and 25μm are especially useful for the identification of molecules via vibrational spectroscopy. As a consequence the wide intrinsic transparency window of chalcogenide glasses (ChGs), which can extend beyond 20μm [1], has created interest in the development of ChG fiber and planar waveguide devices for chemical and biological sensors [2–5]. To improve sensitivity, planar micro-resonators for spectroscopic sensing have been developed [6]. In addition, micro-resonator-based frequency combs are of considerable interest for numerous applications beyond spectroscopy such as precision frequency metrology and optical clocks [7–9].

Optical resonators integrated with planar microfluidic systems have already been demonstrated in the NIR [10–12] and progress in chip-based ChG resonator sensors for biological and chemical sensing in the NIR was reviewed in [13]. Recently, high Q ChG-on-silicon disk resonators and a photonic crystal cavity operating at around 5.2μm were demonstrated [14, 15]. Loaded Q factors of 6×10^4~10^5were measured in As_2Se_3 disk resonators, with a $Ge_{23}Sb_7S_{70}$ over-cladding [14] but, because of the over-cladding, these structures cannot be used for sensing. Cavity-enhanced MIR spectroscopic sensing of chemical molecules was, however, performed using unclad $Ge_{23}Sb_7S_{70}$ disk resonators on a calcium fluoride (CaF_2) substrate, with a loaded Q factor of 1.5×10^4 [16]. In that work micro-disk resonators had to be used due to high waveguide losses (4dB/cm) in the bus waveguides associated with the use of lift-off as the fabrication technology [16]. Micro-disk whispering gallery resonators reduce the interaction of the optical mode with the sidewalls, and this allowed a high intrinsic Q of 2×10^5 at 5.16μm to be achieved [14]. However, a micro-disk also limits the overlap between the optical field and the analyte because of the strong confinement of the optical mode. In comparison waveguide ring resonators can have increased interaction with the analyte, To further increase the field overlap with the analyte, slot waveguides within the ChG rings can be explored as this has the potential to increase the overlap by more than an order of magnitude as has been demonstrated in Silicon [17, 18] and Silicon Nitride slot waveguide based devices [19, 20].

Silicon-on-sapphire (SOS) ring resonators for the MIR have also been studied because this material can have low loss below ~6μm. The first SOS ring resonators operated in the 5.4-5.6μm wavelength range but the waveguide loss was ~4.0dB/cm which limited the Q factors to only 3000 [21]. The highest loaded Q factor of 1.5×10^5 was achieved using grating-coupled SOS ring resonators at ~4.35μm, and this corresponded to a loss of 0.74dB/cm at 4.5μm and an intrinsic Q of 2.78×10^5 [22]. A silicon micro-ring resonator on CaF_2substrate was also reported for MIR spectroscopic sensing [23], but the measured propagation loss of 3.8dB/cm at 5.15μm (corresponding to an intrinsic Q of 6.2×10^4) was too high to use for either slot waveguides or comb generation.

Optical frequency combs based on nonlinear crystals [24], micro-resonators [25–28], and quantum cascade lasers [29] have been demonstrated in the MIR. Chip-based resonators for frequency combs are particularly attractive, since the resonator and the coupling waveguide are monolithically integrated which provides stable coupling even in the presence of vibration and environmental fluctuations [30]. However, chip-based octave spanning frequency combs generated in silicon nitride micro-resonators by pumping at1550nm, reach only the very lower edge of the MIR at 2.4μm [31, 32]. And these are yet to be demonstrated using ChG waveguide resonators.

In this paper, we report the first MIR low loss ChG waveguide ring resonators and demonstrate the lowest propagation losses in a ring beyond 4.5μm for any MIR materials system to date. Loaded Q factors at 5.2μm of up to 58,000were obtained, corresponding to an intrinsic Q of 145,000 and a waveguide propagation loss of 0.84dB/cm.

#240917 Received 18 May 2015; revised 30 Jun 2015; accepted 1 Jul 2015; published 23 Jul 2015

2. Design of chalcogenide ring resonators for MIR sensing

A major challenge in development of MIR waveguide devices is to select a substrate material that has a lower refractive index than the core as well as low optical losses. A reasonably large core-cladding index contrast is also required to allow bending of the waveguides to radii of a few hundred microns or less, and this typically requires an index contrast >0.2. The waveguides should also be single mode. If operation out beyond 10μm is ultimately required, then there are very few materials choices. Whilst CaF_2 crystalline substrates have been successfully employed [16, 23] they are both expensive and extremely fragile. Likewise other materials used as MIR substrates such as Crystran are not generally available in wafer form suitable for planar CMOS style processing. Therefore, it becomes necessary to deposit the lower cladding onto some convenient inexpensive wafer substrate such as silicon. In this work we chose to use a lower index chalcogenide glass with composition $Ge_{11.5}As_{24}S_{64.5}$ as the bottom cladding combining this with a $Ge_{11.5}As_{24}Se_{64.5}$ core material. These compositions are known to deposit with bulk-like glass properties [33] meaning annealing is not required (cracking during annealing is an issue for films thicker than about 1.5μmas are typically required for MIR devices).

The waveguides were modeled using RSoft FEMSim using $Ge_{11.5}As_{24}Se_{64.5}$ glass as the core material upon a $Ge_{11.5}As_{24}S_{64.5}$ glass film as the lower cladding. Ridge or deeply etched rib designs were studied since it allowed the core to be exposed to air (or the analyte) on three sides for sensing purposes. The core refractive index at 5.2μm was 2.595 and the cladding 2.275 as determined using variable angle MIR spectroscopic ellipsometry. The optimum waveguide design had a 2.5μm wide core fabricated from a 2.5μm thick film etched 90-95% of its thickness leaving a thin film of the core glass covering the whole lower cladding. This left a large contact area between the core and cladding improving the adhesion to the substrate and making the waveguide robust to processes such as cleaving. The design was single mode at 5.2μm, shown in Fig. 1(a), and modeling showed that the bend radiation loss was negligible for radii >70μm as illustrated in Fig. 1(b) as the black line. However, the bend radius needed to be >180μmto reduce the junction loss to <0.015dB/junction, (also shown in Fig. 1(b) as the blue line). In this design, therefore, the junction loss was the main contribution to the bend loss.

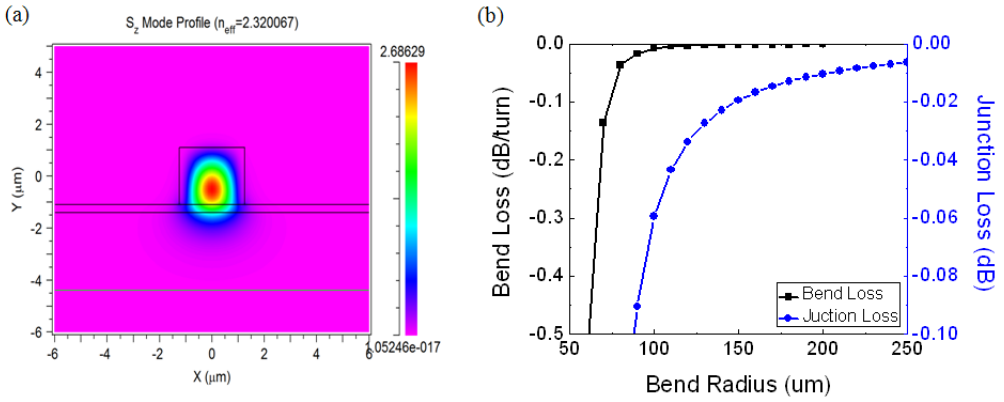

Fig. 1. (a) Mode profile of $Ge_{11.5}As_{24}Se_{64.5}$ waveguide at 5.2μm; (b) Bend loss and junction loss as a function of bend radius.

If the lower cladding were to be deposited directly onto the silicon substrate, radiation losses to the substrate have to be considered because of its very high refractive index. The radiation loss as a function of the lower cladding thickness is shown in Fig. 2 (black line). It is clear that the bottom cladding has to be thicker than10μm to obtain negligible losses. This is a problem from a fabrication perspective as the deposition of such a thick cladding takes a long

#240917 Received 18 May 2015; revised 30 Jun 2015; accepted 1 Jul 2015; published 23 Jul 2015

time and there is a high risk that the film will crack during processing due to the large mismatch in thermal expansion coefficients between the silicon and the chalcogenide glass. Therefore, a substrate based on oxidized silicon wafers was modelled. Whilst silica has significant absorption at 5.2µm, its refractive index is very low and due to the large index contrast with the chalcogenide bottom cladding this results in only very small field penetration into the silica. Figure 2 (blue line) shows the waveguide loss due to absorption in the silica as a function of the thickness of the bottom cladding thickness. With a 3µm layer of $Ge_{11.5}As_{24}S_{64.5}$glass, the propagation loss is ~0.05dB/cm which is acceptable and this is also thin enough to reduce the likelihood of cracking during processing.

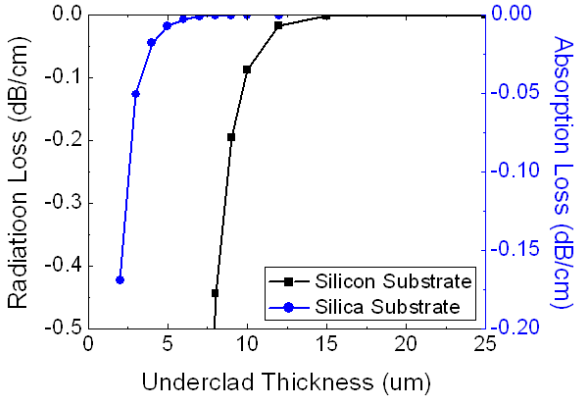

Fig. 2. Radiation loss to silicon substrate and absorption loss of waveguide on silica for variable $Ge_{11.5}As_{24}S_{64.5}$ underclad thickness.

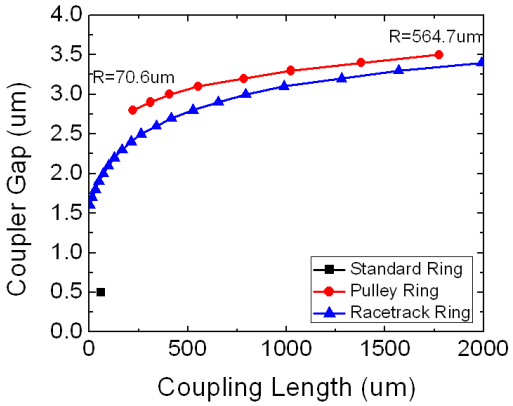

Fig. 3. Coupler gap vs. coupling length of standard, pulley and racetrack coupled ring structure for critical coupling. Loss is assumed 1dB/cm.

The ring design was the last element of the waveguide problem. The most dimensionally critical part of the ring is the coupler, both from the perspective of lithographic resolution and critical dimension tolerance. Several ring structures were considered with the goal being to have the coupler gap no less than 1.5µm such that the devices could be reliably fabricated by low cost contact or 1x projection lithography. Standard bus coupled circular rings, "pulley coupled" circular rings and bus coupled racetrack designs were all considered and modelled to determine the coupler gap required for critical coupling assuming a 1dB/cm waveguide propagation loss. The coupler gap resulting from the required coupling length for critical coupling of the various ring structures are plotted in Fig. 3 modelled using RSoftFEMSim and BeamPROP. The dimension of the waveguides was as above. In the modelling, the ring

#240917 Received 18 May 2015; revised 30 Jun 2015; accepted 1 Jul 2015; published 23 Jul 2015

circumference was varied to change the coupler length meaning that for the standard and pulley coupled designs that the bend radius was varied. For the racetrack, the bend radius was fixed at 180μm, but the length of the straight connecting the 180 degree bends was varied.

For lateral coupling of a standard ring, the effective interaction length is set by the radius of ring and the center-to-center separation [34]. Therefore, only one standard ring structure was obtained in our simulation range, with a minimum coupler gap of 0.5μm, effective coupling length of 58.25μm and band radius of 180μm, shown as a black square in Fig. 3. The gap is too small for reliable printing with non-reduction based optical lithography tools and so was not considered. The "pulley coupled" rings also have the coupling length set by the bend radius, and radii varying from 70 to 600μm are shown in red circles in Fig. 3, providing only a modest gain in coupler gap over the racetrack design.

The Racetrack coupled ring structure was chosen for two reasons. Firstly it does not preclude the use of an Add/Drop architecture in future devices whereas the pulley device makes this impossible. Secondly, although the "pulley coupled" ring structure enables a slightly wider coupling gap than racetrack structure, the larger bend radius for a fixed ring length and the need for a return bend to route the waveguides to opposing facets on the chip means more chip height is required for each ring, limiting the potential integration density and number of devices per die/wafer. The racetrack however suffers from the need for four bend transitions leading to increased ring losses, though this is offset to a degree by the lower curved section length where the waveguide losses are typically higher due to remnant rasterization noise on the waveguide sidewalls. The junction losses can also be eliminated by the use of adiabatic bends [35]. The choice of a racetrack design meant that the minimum ring size was set by the coupler length and the allowable bend radius, resulting in a ring with length ~2mm and expected free spectral ranges in the 1-2cm^{-1} range, adequate for many spectroscopy applications whilst remaining reasonably compact.

A photomask was then laid out, and to account for uncontrolled variations of material refractive indexes, dimensional tolerances in the waveguide processing, and uncertainty in the waveguide loss, the coupler gap was varied between 1.5 and 3.5μm in steps of 0.5μm and the coupler length between 250 and 600μm in 50μm steps. This provided ring lengths of 1.631mm to 2.331mm in 100μm steps, and the mask design was created using a custom technology node for our waveguide set up in IPKISS [36]. The mask was then fabricated by Taiwan Mask Corporation using a process that optimized the line edge roughness on both the straight and curved sections of the design to minimize raster induced sidewall roughness losses.

The last design element revolves around the waveguide end facets. Strong Fabry-Perot effects were observed with MIR external cavity tunable quantum cascade lasers (QCL) when measuring low loss chalcogenide waveguides [37]. An antireflection (AR) coating for resonator samples is crucial to reduce the quite large parasitic cavity effects that can otherwise make measurements of the ring response difficult. Plasma Enhanced Chemical Vapour Deposited (PECVD) fluoropolymer is a good choice as an AR coating for the lower part of the MIR spectrum. Figure 4(a) shows the calculated plane wave facet reflection of the waveguides with a fluoropolymer coating. The AR coating optimum for 5.1μm is a 950nm layer of fluoropolymer shown as Fig. 4(b). The refractive index of the fluoropolymer was measured at 1.35 as determined from a variable angle scanning MIR ellipsometer. The reflection can thus be reduced to 1.3% from the ~16% starting point.

#240917 Received 18 May 2015; revised 30 Jun 2015; accepted 1 Jul 2015; published 23 Jul 2015

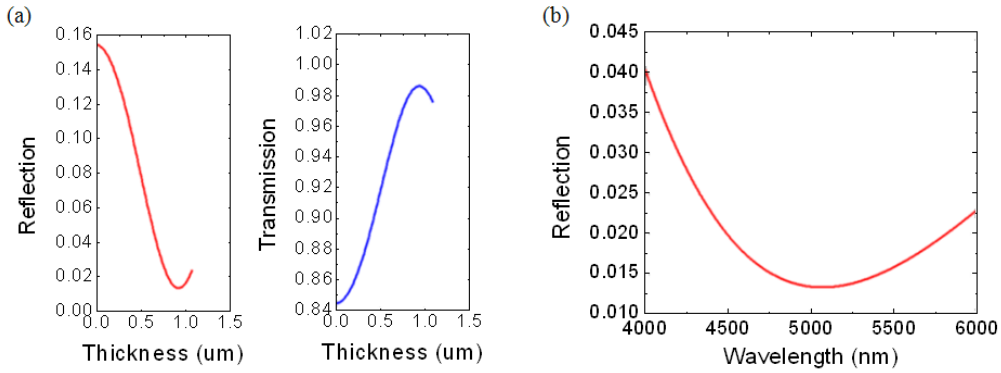

Fig. 4. (a) Reflection and transmission vs. fluoropolymer thickness at 5.1μm; (b). Reflection of waveguide end facet with fluoropolymer coating 950nm thick as a function of wavelength.

3. Experiments

3.1 Fabrication of high-Q chalcogenide MIR ring resonators

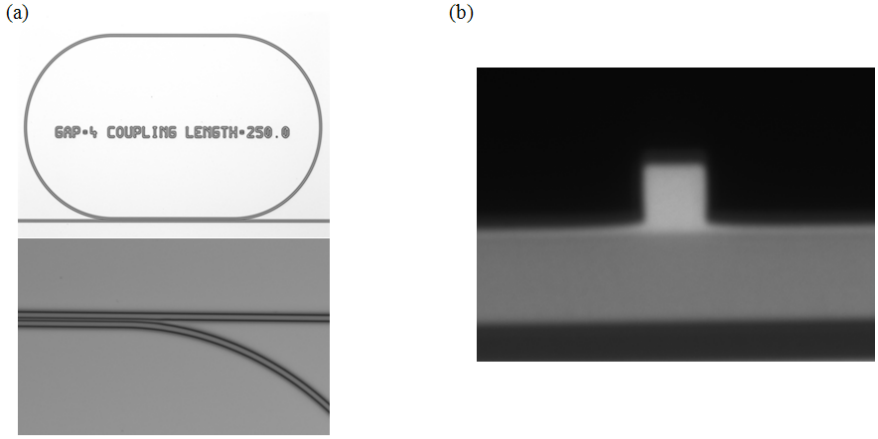

Fig. 5. (a) Optical microscope top-view image of a 180 μm radius MIR resonator; (b) Cross section image of the waveguide.

$Ge_{11.5}As_{24}Se_{64.5}$and $Ge_{11.5}As_{24}S_{64.5}$ films were deposited via thermal evaporation onto thermally oxidized silicon (TOx) wafers using an Angstrom Engineering deposition system. A 3μm thick $Ge_{11.5}As_{24}S_{64.5}$ bottom cladding followed by a 2.5μm thick $Ge_{11.5}As_{24}Se_{64.5}$ core layer was deposited onto a silicon wafer with a thick 5μm TOx layer. Measurement of the surface roughness of the top of the core layer using an interference microscope revealed an RMS roughness of <0.6nm, a figure more than adequate for the proposed waveguide design. Resonator patterns were then formed on the film using standard positive photoresist technology exposed with a Canon MPA500 1x projection aligner followed by standard wet development. The ChG core layer was then dry-etched using an inductively coupled plasma reactive ion etcher (Oxford Instruments Plasmalab ICP100) with CHF_3 gas as described in [38]. The residual photoresist layer was removed using wet chemical stripping and oxygen/argon plasma etching. The top surface of the waveguides was covered with a 10nm thick fluoropolymer layer, which prevents surface chemisorption of hydrocarbon and water contaminants [37]. Figure 5(a) shows the top view of a racetrack-coupled MIR ring resonator, and Fig. 5(b) shows a cross section image of the waveguide. After cleaving, a 950nm

#240917 Received 18 May 2015; revised 30 Jun 2015; accepted 1 Jul 2015; published 23 Jul 2015

fluoropolymer layer was deposited on both end faces using PECVD with CHF_3 as the feed gas [39].

3.2 MIR measurement setup

To measure the performance and demonstrate the ability of these resonators for spectroscopy, we employed the apparatus shown in Fig. 6. Here a tunable 5.2μm QCL (Daylight Solutions, Inc.) was used as the source both in scanning mode and also in externally driven PZT tuning mode for high resolution measurements around the resonance dips over a ~2.6nm range.

A 2.5cm thick ZnSe crystal with parallel polished faces was set in a tap off from the beam path as a frequency reference for scan linearity compensation, which was used to calibrate the FWHM of the resonators. Three DC coupled cooled MCT detectors (VIGO System S.A.) were used as power monitor, frequency reference and resonator signal respectively. Data acquisition and system control was achieved using a custom LabView program and 16bit data acquisition cards. Combined with this program, this set up provided a fine scan with sub-pm resolution and accuracy for resonator testing. In the measurement, light was coupled into the waveguides using a molded chalcogenide aspheric lens with NA = 0.85. The light emerging from the resonators was collected with a NA = 0.56 chalcogenide lens and either imaged onto a Xenics Onca InSb camera which was used to optimize alignment, or detector 1 in Fig. 6.

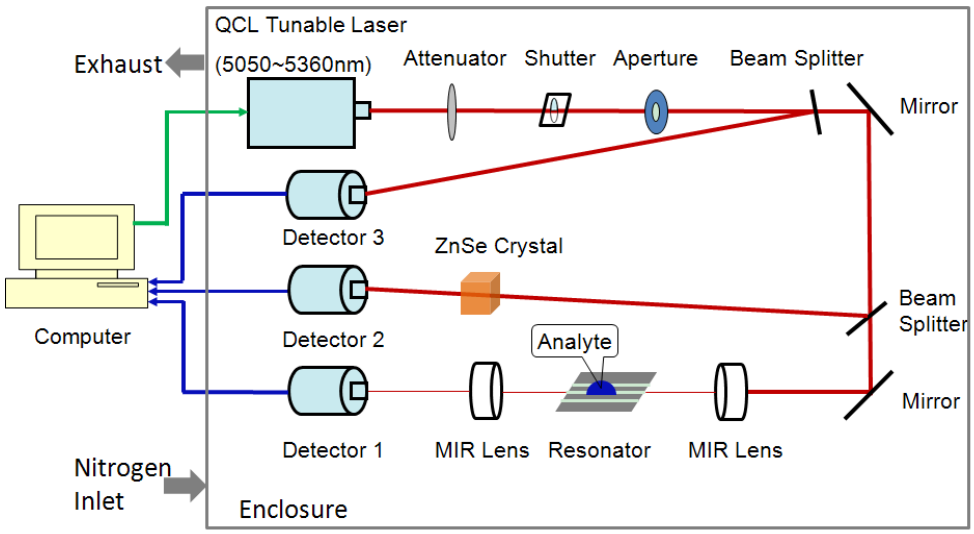

Fig. 6. Schematic of MIR measurement apparatus.

4. Results and discussion

The impact of the AR coating was first ascertained on reference waveguides. The transmission spectra of waveguides with and without AR coating are shown in Fig. 7. The contrast of the Fabry-Perot fringes was significantly reduced from 1.7 to 1.1 with the AR coating, which significantly eased subsequent resonator measurements. The remnant low frequency oscillation came from a Fabry-Perot resonance within the QCL itself.

The resonator performance was next measured. A 1.3 cm long sample coated with 10nm fluoropolymer layer was aligned in the setup. Resonators with different coupling gap and length were measured. Additionally, a reference straight waveguide adjacent to the resonator under test and with the same structure as the bus waveguide of the resonator was also measured to enable complete removal of the residual Fabry-Perot fringes for each measurement by post processing.

#240917 Received 18 May 2015; revised 30 Jun 2015; accepted 1 Jul 2015; published 23 Jul 2015

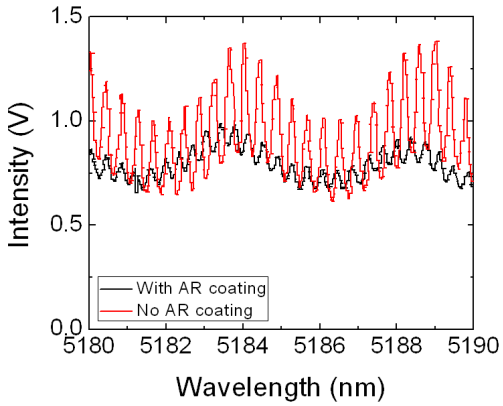

Fig. 7. Transmission spectra of reference waveguides with and without 950nm fluoropolymer AR coating (not normalized for QCL power variations).

Figure 8(a) shows the TE polarization transmission spectrum of the highest extinction resonator measured with the QCL in sweep mode. The group index calculated from the Free Spectral Range experimentally measured ~5.28nm was 2.77, which is consistent with our Rsoft simulation result 2.765.Accurate characterization of the resonators however had to be undertaken using the piezo tuning mode of the QCL due to sweep mode wavelength being non-monotonic which lead to uncertainties about the precise wavelength scale. The piezo scan avoided this issue though with a significantly nonlinear wavelength scan. The ZnSe reference cavity in Fig. 6 was used to eliminate this nonlinearity using custom correction software. Figure 8(b) shows the spectrum measured from the highest extinction device after removing the residual F-P fringes, normalization and sweep linearization. The −3dB bandwidth of the resonance dip was 0.089nm, leading to a loaded Q factor of 5.8×10^4. Based on measurements of the other devices we established which side of critical coupling the response was measured, and then by fitting of the results to a standard ring model we obtained an intrinsic Q factor of 1.45×10^5 for the best resonators and a waveguide propagation loss of 0.84dB/cm after backing out the expected 0.06dB of bend junction loss in the ring. Losses varied in the range 0.84-1.03 dB/cm measured over multiple sets of resonators. In this case, the power input to the waveguide was ~1mW, as the resonators displayed clear thermal behavior at higher input power. The thermal behavior of micro-cavity systems presents as a shift of the resonance wavelength and an asymmetric spectrum shape [40], which is just starting to become apparent in Fig. 8(b). No resonance splitting is visible in the measured result suggesting low scattering to backward propagating modes.

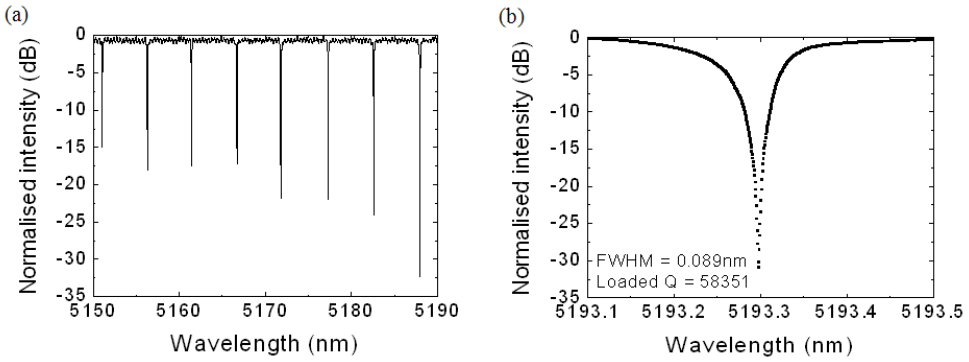

Fig. 8. (a) MIR optical transmission spectrum of the racetrack resonator measured with QCL sweep mode; (b) Spectrum near the optical resonance at 5193.3nm.

#240917 Received 18 May 2015; revised 30 Jun 2015; accepted 1 Jul 2015; published 23 Jul 2015

The propagation loss of the bus waveguides was also measured separately by the "cut-back" method by using reference waveguides present with each set of rings on three chips of different lengths from the same wafer. The insertion loss data for these chips is presented in Fig. 9 from which a propagation loss of 0.60 ± 0.08dB/cm was calculated at 5.2μm, where the error figure represents the highest and lowest slope lines passing through the data points. This is a lower figure than that observed in the rings and the difference exceeds the size of the estimated errors in the measurements and so is deemed significant.

The loss figure of 0.84dB/cm is nonetheless the lowest value reported in MIR ring resonators in the >4.5μm wavelength band to the best of our knowledge. The propagation loss is slightly higher than the lowest waveguide loss values reported in chalcogenide rib waveguides in the MIR (0.4dB/cm at 5.2μm) [37], due to a narrower ridge and greater etch depth in the waveguides employed in the resonator. Whilst the losses and consequent Q factors achieved are likely sufficient for sensing applications they are not yet good enough for comb generation using pumps at ~5μm in the anomalous dispersion region of chalcogenide glasses. This requires higher Q factors than devices pumped at shorter wavelengths as the waveguide nonlinearity γ is proportional to n_2/A_{eff} and the effective mode area A_{eff} is large at longer wavelengths whilst the material nonlinear index n_2 is falling due to dispersive effects. Consequently the loss still needs to be somewhat lower for MIR comb generation.

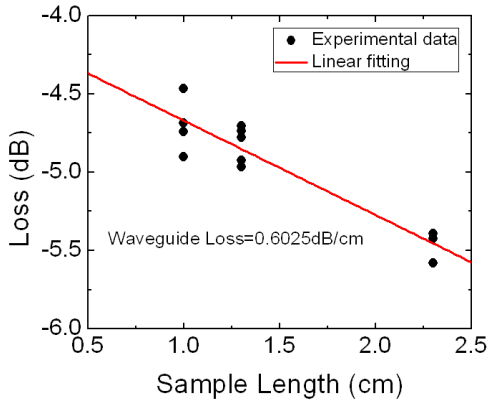

Fig. 9. Insertion loss data and linear least square fitting estimate of propagation loss for three separate chips with straight waveguides at 5.2μm.

Calculation using an effective index implementation of the Payne-Lacey model [41] indicated that the scattering loss for the air clad waveguides should be below 0.2dB/cm for the observed sidewall roughness in these waveguides and even lower for chalcogenide clad devices. Measurement of the propagation losses at 1550nm gave a propagation loss of 1.7dB/cm confirming that the propagation loss did not follow the expected $1/\lambda^2$ trend moving from 5.2 to 1.55μm, and further suggesting that the measured propagation loss at 5.2μm is not due to sidewall roughness induced scattering. The exact nature of the loss mechanism and the reasons for the propagation loss differences in the rings compared to the straights is under further study with the goal of attaining Q factors around 10^6 in this region of the MIR as required for comb generation.

5. Conclusions

A fabrication-tolerant design methodology and implementation details for chalcogenide waveguide based ring resonators operating in the 5.2μm region of the MIR spectrum have been presented. Based on this, ring resonators with an air top cladding have been fabricated and tested demonstrating loaded Q factors~6×10^4 corresponding to intrinsic Q factors up to 1.45×10^5. A waveguide propagation loss of 0.84dB/cm in the ring was deduced and straight

#240917 Received 18 May 2015; revised 30 Jun 2015; accepted 1 Jul 2015; published 23 Jul 2015

waveguide losses of 0.60dB/cm measured, both limited by effects other than sidewall scattering loss. This Q factor is amongst the highest values ever reported in experimentally demonstrated mid-IR resonators, and the best at wavelengths >5μmas are the observed propagation losses. These resonators can be used for cavity-enhanced MIR spectroscopy and with further loss reduction will lead to potentially octave spanning frequency comb generation from an integrated device in the >5μm region for the first time.

Acknowledgments

Pan Ma acknowledges the financial support from the China Scholarship Council for her joint PhD Scholarship No. 201206020094. Yi Yu acknowledges the financial support from the China Scholarship Council for her PhD Scholarship No.201206110048. This research was conducted under Australian Research Council (ARC) Centre of Excellence for Ultrahigh Bandwidth Devices for Optical Systems (project number CE110001018). Dr. Duk-Yong Choi is supported by ARC Future Fellowship FT110100853. Device fabrication was supported by the ANU node of the Australian National Fabrication Facility (ANFF).

#240917 Received 18 May 2015; revised 30 Jun 2015; accepted 1 Jul 2015; published 23 Jul 2015